

Fibre Diffraction Spot Profiles and the Lorentz Correction

Richard Denny

Biophysics Section, Blackett Laboratory, Imperial College,
London SW7 2BZ &
CCLRC Daresbury Laboratory, Warrington WA4 4AD.

Introduction

When introducing users to the integration of fibre diffraction intensities using the program LSQINT, the following questions frequently arise:

- i) Does LSQINT apply the Lorentz correction?
- ii) How does it do it?
- iii) What happens at the meridian?

The short answer is that it is all taken care of in the profile calculation but perhaps further explanation would be useful.

The Lorentz correction can be thought of as having two components, the smearing out of Bragg-sampled intensities into annuli due to cylindrical averaging of the intensity transform and the oblique intersection of these annuli with the sphere of reflection. The latter component is dealt with by correct transformation of the image into reciprocal space [1]. However, the first component of the correction still requires attention and that is what is discussed here.

The model fibre

In general, the orientation of a three-dimensional object is specified by three angles, two of which define the orientation of the particle axis and one which defines the orientation of the particle about its own axis. An orientation distribution function (ODF) describes the probability of finding a particle in a given orientation. In an ideal fibre, the particles are assumed to be the same size and cylindrical, with no correlation between the positions of neighbouring particles. The particle axes are distributed about the fibre axis in a cylindrically symmetric manner and for a given orientation of the particle axis, all orientations about the axis occur with uniform frequency, so that the orientation distribution function is dependent on only one angle (figure 1). The particles might exhibit one or three-dimensional crystallinity. Three dimensional crystallinity results in a polycrystalline fibre, giving rise to Bragg-sampled intensity.

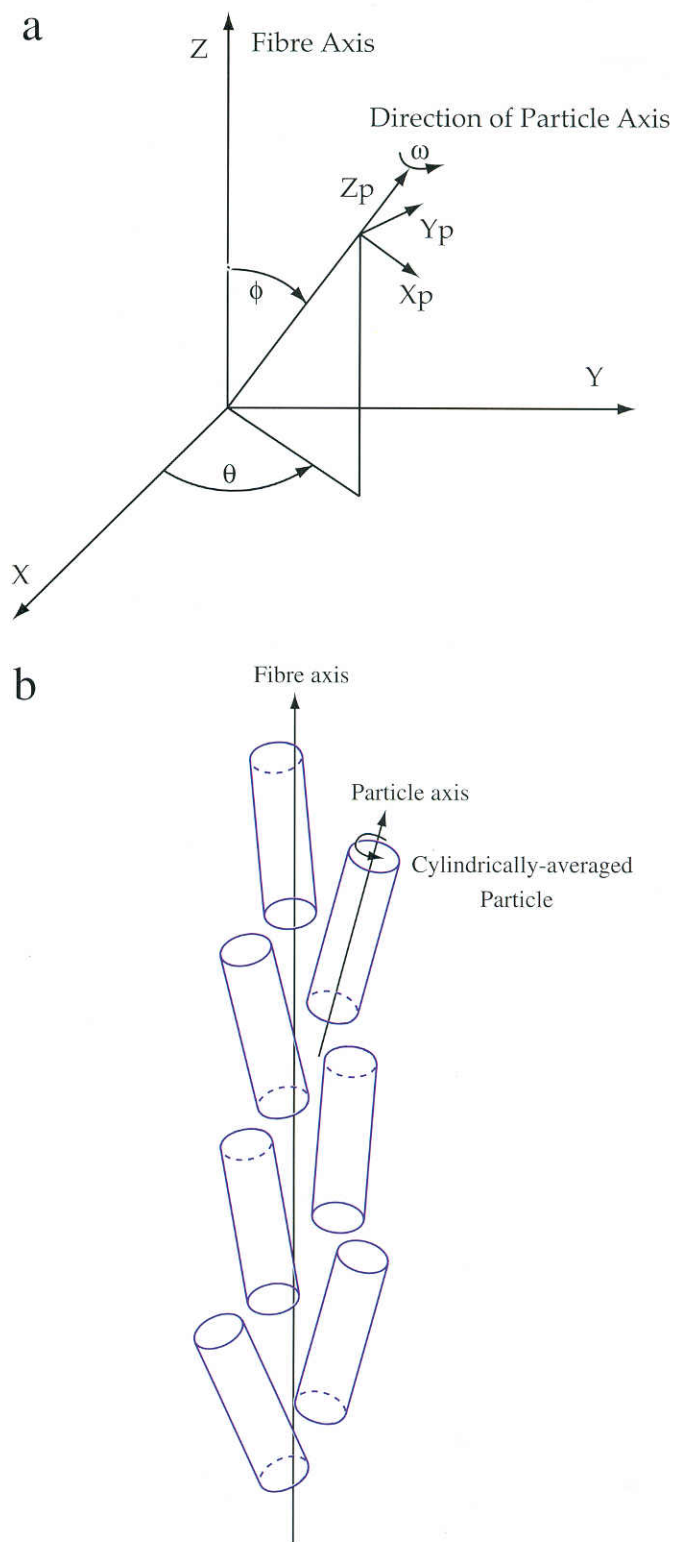


Figure 1: The diagram in (a) shows the angles used to describe the orientation of a particle in three dimensions; the direction of the particle axis is specified by θ and ϕ , while the orientation of the particle and its internal coordinate system about this axis is specified by ω . The diagram in (b) shows a representation of an ideal fibre. All the particles constituting the fibre are cylindrical and of the same size. All values of θ are equally likely, as are all values of ω , so that the orientation distribution function can be written as function of ϕ alone.

Diffraction from a crystalline particle

A diffraction spot from a single particle will have a breadth which is reciprocally related to the particle

size. In general, the Fourier transform of the shape function of the particle $S_{lat}(\mathbf{D})$, is convoluted with the reciprocal lattice $L(\mathbf{D})$, to give the Fourier transform of the finite lattice. This is then squared to give the interference function, *i.e.*

$$Z(\mathbf{D}) = |L(\mathbf{D}) \otimes S_{lat}(\mathbf{D})|^2$$

where \mathbf{D} is a reciprocal space vector. If the $S_{lat}(\mathbf{D})$ on each reciprocal lattice point do not overlap significantly, this can be simplified [2] to

$$Z(\mathbf{D}) = \frac{1}{V_{cell}} [L(\mathbf{D}) \otimes |S_{lat}(\mathbf{D})|^2]$$

For a cylindrical particle, the spot shape can be modelled reasonably well with a Gaussian for the spread in the Z direction and another Gaussian for the radial spread, with widths w_z and w_R , respectively. The particle intensity transform at a point in a cylindrical coordinate system can now be written as,

$$I(R_p, \psi_p, Z_p) = \frac{1}{\pi^{3/2} w_z w_R^2} \sum_{hkl} I_{hkl} e^{-R^2/w_R^2 - (Z_1 - Z_p)^2/w_z^2}$$

where $R^2 = R_p^2 + R_l^2 - 2R_p R_l \cos(\psi_p - \psi_l)$. The broadening function has been normalized so that, in practice, it is easy to compare integrated intensities from lattices with different degrees of broadening.

This distribution of intensity can be cylindrically averaged, consistent with the requirements of the model that for a given orientation of the particle axis, particles can be found with equal probability at any orientation about that axis,

$$\langle I(R_p, \psi_p, Z_p) \rangle_{\psi_p} = \sum_{hkl} \frac{m_{hkl}}{2\pi \cdot \pi^{3/2} w_z^2 w_R^2} \int_0^{2\pi} I_{hkl} e^{-[R_l^2 + R_p^2 - 2R_l R_p \cos(\psi_p - \psi_l)]/w_R^2 - (Z_1 - Z_p)^2/w_z^2} d\psi_p$$

This gives the equation for the cylindrically averaged particle intensity transform (CAPIT),

$$I(R_p, Z_p) = \frac{1}{\pi^{3/2} w_z^2 w_R^2} \sum_{hkl} m_{hkl} I_{hkl} e^{-(R_l - R_p)^2/w_R^2 - (Z_1 - Z_p)^2/w_z^2} i_0(2R_p R_l/w_R^2)$$

where $e^x i_0(x) = I_0(x)$, a modified Bessel function.

Here, the summation has been modified to be over the unique intensities and a multiplicity, m_{hkl} associated with each unique reflection has been introduced. This arises as there is systematic overlap of reflections (which are not necessarily symmetry related) due to the cylindrical averaging (figure 2).

The cylindrical averaging performed above implicitly provides the velocity component of the Lorentz correction. Figure 3 shows the effect of the averaging on the maxima of diffraction spots of three different widths at varying radii. Curves

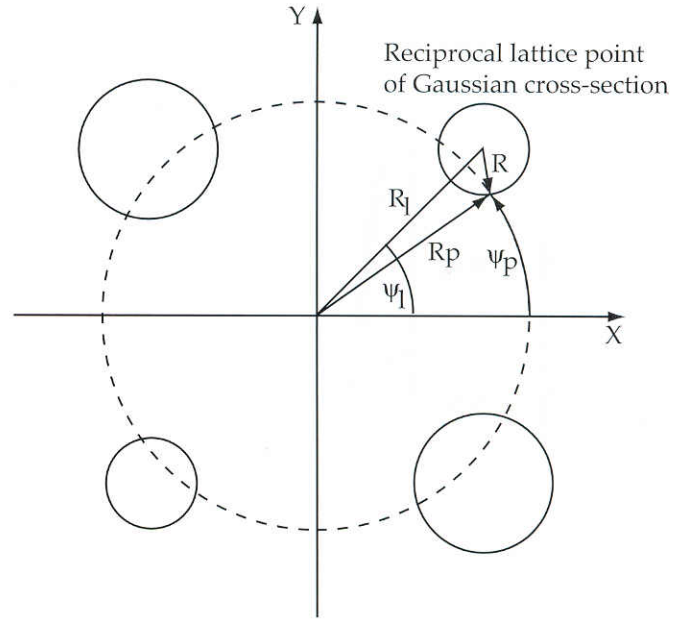


Figure 2: The reflections are assumed to be of Gaussian cross-section (the different sizes of the circles indicates that cylindrical averaging may sum contributions from reflections which are not symmetry related and so are of differing intensity). (R_l, ψ_l) are the coordinates of the lattice point and (R_p, ψ_p) is the point in the particle transform at which the contribution of this lattice point is being considered. The contribution at all points of equal radius must be summed to obtain the cylindrically averaged particle intensity transform.

corresponding to $1/R$ scaled to match the curves calculated from the CAPIT equation, are also shown for comparison. It is clear that the fall-off of intensity depends on the width of the spot. It is also clear that the $1/R$ curve is a better approximation at smaller widths at a given reciprocal radius or larger radii for a given width. The meridian is well-behaved with the averaging approach, the maximum of a spot having the same value it would have if the particle were not cylindrically averaged. This is of course not the case when applying the $1/R$ curve, where the traditional Lorentz correction breaks down completely.

How a point in the particle intensity transform contributes to the specimen intensity transform

So far, only one component of the orientation distribution function has been considered; the cylindrical averaging of each particle about its own axis. In order to calculate the specimen intensity transform, the remaining components of the ODF are convoluted with the intensity distribution from a single particle. As the distribution of particle axes about the fibre axis is cylindrically symmetric, only the dependence on ϕ need be considered. This is achieved by choosing the vector to the desired point in the specimen intensity transform as the axis about

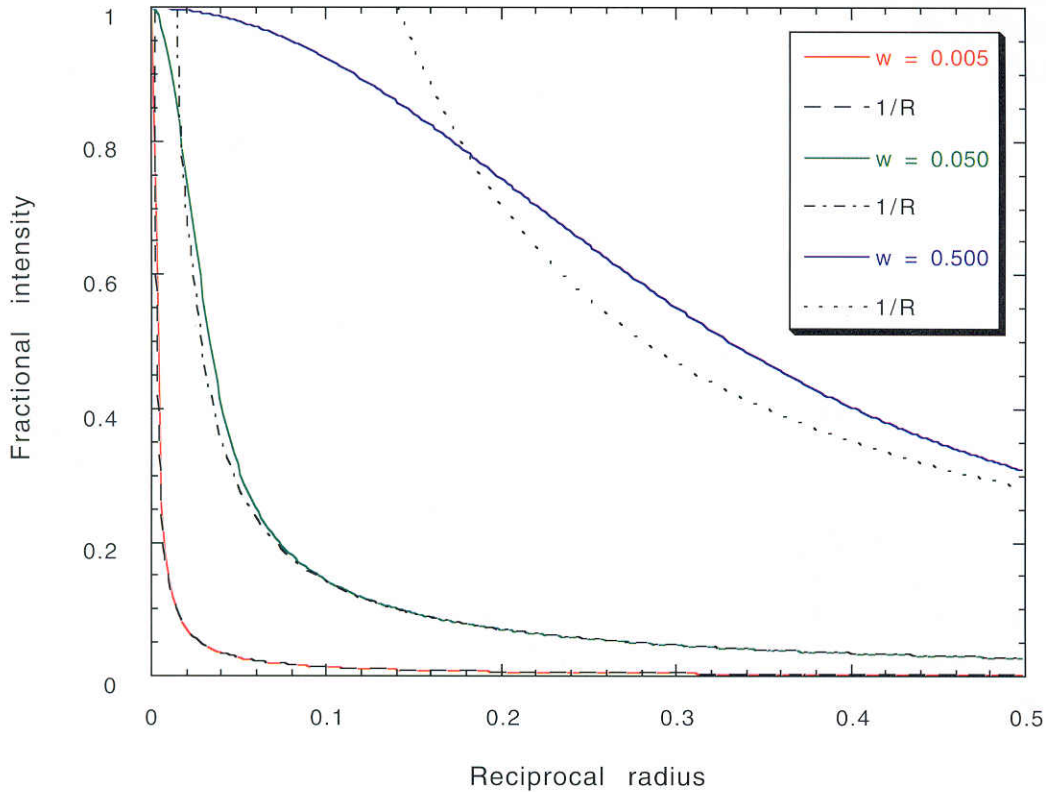


Figure 3: This graph shows the effect of cylindrical averaging reflections. The Y axis is the peak intensity of the averaged reflection as a fraction of its peak value in the three-dimensional particle coordinate system. The red, green and blue curves are the result of applying the CAPIT equation to the situation where $R_p = R_r$, between values of 0.0 and 0.5 on an arbitrary scale for different widths of the Gaussian cross-section of the reflections. The three broken curves show the function $1/R$ scaled to match the curves derived from the CAPIT equation. The coloured curves all intersect the Y axis at 1.0 indicating that meridional reflections have the same peak value in the cylindrically-averaged intensity transform as they have in the three-dimensional

which to integrate (see figure 4). First we consider all those particle axes which will make the same contribution to this point in the specimen transform. These particle axes will form a cone around the axis of integration. We must multiply each point on the base of the cone by the probability of finding a particle axis at that orientation according to the ODF. We can then integrate over all possible cones to complete the convolution [3], *i.e.*,

$$I(D_s, \sigma_s) = \int_0^\pi I(D_p, \sigma_p) \sin \sigma_p \int_0^{2\pi} N(\phi) d\xi d\sigma_p$$

where $\cos \phi = \cos \sigma_s \cos \sigma_p + \sin \sigma_s$ and $D_p = D_s$.

The effect of this convolution is to smear the diffraction spots out into arcs. The extent of the arcs modifies the Lorentz correction one would apply to the peak intensity of the diffraction spot. In terms of a traditional Lorentz correction, the fall-off of intensity would go from being proportional to $1/R$ for perfect orientation of the particle axes parallel to the fibre axis to being proportional to $1/D^2$ for powder type disorientation where the particle axes are randomly oriented with respect to the fibre axis. Again, this correction is implicit in the above

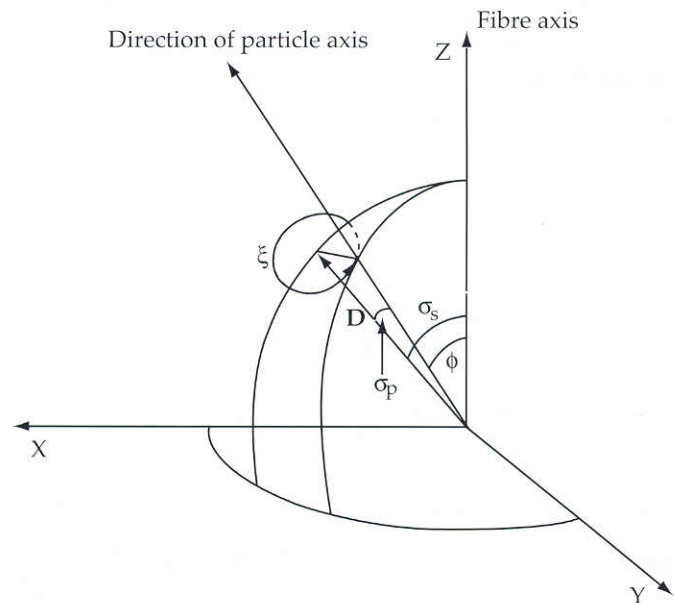


Figure 4: The convolution of the cylindrically-averaged intensity transform with the remaining components of the orientation distribution function (in θ and ϕ) calculated at a point (D, σ_s) . All particles making the same contribution to this point (*i.e.* all particles whose axes are σ_p away from the vector \mathbf{D}) are summed by integrating over ξ . The integration is then performed over σ_p .

convolution which deals comfortably with the situation where broad diffraction spots lie close to the meridian or the centre of the pattern.

Conclusion

If the traditional form of the Lorentz correction is applied to diffraction spots on a point by point basis, a good approximation to the profile calculation described above is obtained when the spots are not too close to the meridian. However, this method of correcting spot intensities breaks down at the meridian and works poorly where broad spots lie close to the meridian. The method employed by LSQINT naturally applies to these situations and also provides an easy way of scaling together diffraction spots of different widths, possibly from different structures within the same specimen.

References

- [1] Fraser, R.D.B., Macrae, T.P., Miller, A. and Rowlands, R., (1976). *J. Appl. Cryst.* **9**, 81-94.
- [2] Stroud, W.J. and Millane, R.P. (1995). *Acta Cryst.* **A51**, 771-790.
- [3] Holmes, K.C. and Barrington Leigh, J. (1974). *Acta Cryst.* **A30**, 635-638.

3-D Reconstruction from Fibre X-ray Diffraction Patterns: Myosin-Decorated Actin Filaments

J.J.Harford¹, R.C.Denny¹, E.Morris², R.Mendelson³ and J.M.Squire¹

¹ Biophysics Section, Blackett Laboratory, Imperial College, London;

² Biochemistry Department, Imperial College, London

³ Cardiovascular Research Institute, UCSF, San Francisco.

Helical biological particles such as actin filaments have been studied for many years by electron microscopy and their structures have been determined to about 20Å to 30Å resolution by 3-D reconstruction from single images [1,2]. A big advantage of electron micrographs is that they are real space images of the objects being studied. If one uses methods of reconstruction based on Fourier transforms computed from digitized images, then both amplitude and phase information can be obtained. A single view of a helical object contains many images of the repeating unit on the helix but

with different rotations around the helix axis. Therefore, a single view is sufficient to reconstruct the full helix in 3-dimensions. The main problems with electron microscopy of such biological filaments (often contrasted by using negative staining methods) are that the resolution is usually limited to about 20Å and the amplitude data are uncertain because of the contrast transfer function of the electron microscope.

X-ray fibre diffraction studies from equivalent systems can have the advantage that the diffraction information can extend to about 10Å and beyond and, when properly stripped, the layer-line data should be reliable. However, unlike electron microscopy data, there is little phase information and one cannot directly compute a 3-D reconstruction. This paper discusses the combination, to 27Å resolution, of amplitudes from fibre X-ray diffraction patterns of actin filaments labelled with myosin heads (myosin S1) and phases determined from electron microscopy. It also shows how the structure might be refined to a resolution of at least 13Å, far beyond current electron microscopy data, by modelling using the lower resolution reconstruction shown here as a starting point.

During muscle contraction, force and movement are supposed to be produced by the interaction of the globular heads of myosin molecules with adjacent, helical, actin filaments. The myosin heads are known as ATPases; they bind and can hydrolyse the molecule adenosine triphosphate (ATP) to adenosine diphosphate (ADP) and inorganic phosphate (Pi). This hydrolysis is associated with the release of free energy which is utilised to drive the generation of force and movement. The myosin ATPase is rather slow unless the myosin heads are interacting with actin filaments. In the absence of ATP or ADP, the myosin heads become rigidly attached to actin in the so-called rigor complex. This occurs on death when we stop making ATP and our muscles become 'cross-linked', hence stiff (*rigor mortis* sets in), by the permanent binding of myosin heads to actin.

The myosin molecule is a long (1500Å) coiled-coil α -helical rod on one end of which are two myosin heads. The myosin heads can be separated from the rod by proteolysis, yielding individual, isolated, heads known as myosin subfragment-1 (S1). Such myosin S1 molecules can attach to isolated actin filaments in the absence of ATP to form so-called 'decorated' actin filaments. These have a